Eur. Phys. J. Appl. Phys. (2016) 75: 24707
DOI: 10.1051/epjap/2016150587

THE EUROPEAN PHYSICAL JOURNAL APPLIED PHYSICS

Regular Article

Monitoring the removal of excited particles in He/Ar/H_2 low temperature afterglow plasma at 80–300 K*

Ábel Kálosi[1], Petr Dohnal[1], Lucie Augustovičová[2], Štěpán Roučka[1], Radek Plašil[1], and Juraj Glosík[1,a]

[1] Department of Surface and Plasma Science, Faculty of Mathematics and Physics, Charles University in Prague, 18000 Prague, Czech Republic
[2] JILA, University of Colorado and National Institute of Standards and Technology, 80309-0440 Boulder, Colorado, USA

Received: 30 November 2015 / Received in final form: 14 January 2016 / Accepted: 20 January 2016

Abstract. Stationary afterglow (SA) experiments with cavity ring down absorption spectrometer (cw-CRDS) have been used to study recombination of H_3^+ ions with electrons. To characterize the plasma during the afterglow we monitored the time evolution of density of He_2 excited dimers ($a^3\Sigma_u^+$) in plasmas in pure helium and in helium with small admixture of Ar and H_2. By monitoring the plasma decay and its dependence on [H_2] and [Ar] in the afterglow in pure He and in He/Ar/H_2 mixture we estimated the rate of plasma thermalization in the temperature range of 80–300 K. The inferred deexcitation rate coefficients for reaction of helium metastable atoms with H_2 were $(0.9 \pm 0.3) \times 10^{-10}$ cm^3 s^{-1}, $(1.9 \pm 0.2) \times 10^{-10}$ cm^3 s^{-1} and $(2.7 \pm 0.2) \times 10^{-10}$ cm^3 s^{-1} at 80 K, 140 K and 300 K, respectively. The effective recombination rate coefficients for H_3^+ were evaluated from the decay of the electron number density. We propose the lower estimate for the saturation of the effective recombination rate coefficient in H_3^+ and D_3^+ dominated plasma.

1 Introduction

Recombination of H_3^+ ions with electrons at low temperature is important for theoretical physics, physical chemistry, plasma physics, and it is of special interest for astrophysics, because H_3^+ is the most abundantly produced molecular ion in the Universe [1] that plays a key role in the chemistry of the interstellar medium [2]. Because of its importance, it was studied many times, but there were many discrepancies in the results [3]. The binary recombination of H_3^+ ions was studied in merged electron-ion beam experiments [4,5] and in several afterglow experiments [3,6–9]. In afterglow experiments used for studies of H_3^+ recombination the helium buffer gas is used to inhibit diffusive losses and to thermalize the electrons. Hydrogen is the precursor gas for H_3^+ formation, and argon is added to remove undesired He metastable atoms created during the discharge [3,8]. Some experiments were carried out also in pure H_2 [10–12]. Using stationary afterglow (SA) and flowing afterglow with Langmuir probe (FALP) experiments we recently demonstrated that recombination in H_3^+ dominated low temperature plasmas depends on the pressure of the ambient gas. We observed that already at He pressures of 100–2000 Pa, the ion losses due to binary and ternary recombination processes are comparable. This is an unexpected result since the generally accepted classical theory of Bates and Khare [13] predicts such effects at pressures at least by three orders of magnitude higher. To study the ternary recombination processes the afterglow experiments have to be carried out over a large scale of pressures and for various compositions of gases. Because of the dependence of H_3^+ recombination process on many parameters, the afterglow plasma has to be characterized very precisely. It is essential to create experimental conditions at which the afterglow plasma is in thermal equilibrium characterized by the temperature of the buffer gas.

This paper presents the results of the study of plasma thermalization at conditions used for the study of H_3^+ recombination at low temperature and high pressures. The plasma thermalization was monitored by measuring the relative populations of molecular He_2 metastables and excited states of atomic Ar in the temperature range of 80–300 K. We also present and summarize the results of the measurements of binary and ternary rate coefficients of H_3^+ recombination in afterglow plasmas.

2 Experimental

The experiments were performed using a stationary afterglow apparatus combined with continuous wave

[a] e-mail: juraj.glosik@mff.cuni.cz

* Contribution to the topical issue "6th Central European Symposium on Plasma Chemistry (CESPC-6)", edited by Nicolas Gherardi, Ester Marotta and Cristina Paradisi

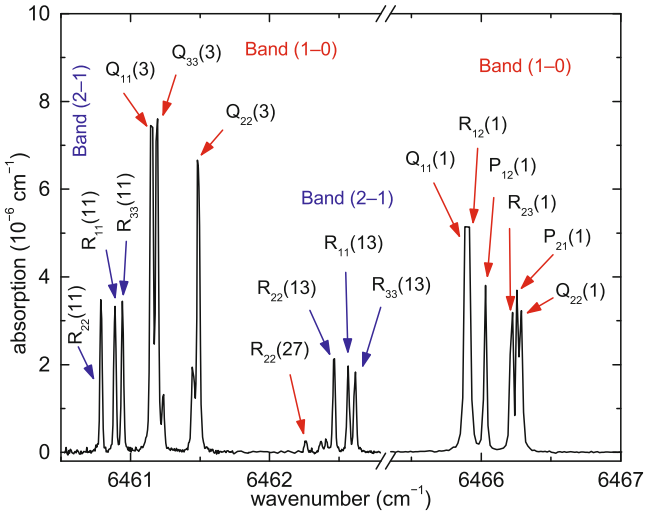

Fig. 1. Observed absorption spectrum of He_2 in the near-infrared spectral region: 6460.5–6467 cm^{-1}. The absorption lines belong to the (1–0) and (2–1) vibrational bands of the $b^3\Pi_g$–$a^3\Sigma_u^+$ system. The measurement was performed during the discharge at 80 K in a He/Ar/H_2 mixture ($8\times10^{17}/10^{14}/2\times10^{14}$ cm^{-3}). The lines are labelled with the corresponding quantum numbers $\Delta J_{F'F''}(N'')$, where $F = 1$ for $J = N + 1$, $F = 2$ for $J = N$, and $F = 3$ for $J = N - 1$ and the prime and double prime denote the upper and lower state, respectively.

cavity ring down spectrometer (SA-CRDS), for detailed description see e.g., references [14,15]. In the experiments the plasma is formed in a pulsed microwave discharge (2.45 GHz, 5–15 W) in a mixture of He/Ar/H_2 (typical composition $\sim 10^{17}/10^{14}/10^{14}$ cm^{-3}), in a mixture of He/Ar ($\sim 10^{17}/10^{13}$ cm^{-3}), in pure He ($\sim 10^{17}$ cm^{-3}), or in pure H_2 ($\sim 10^{16}$ cm^{-3}). Only normal H_2 was used in the experiments. Two fiber-coupled distributed feedback (DFB) laser diodes (1529.55 nm and 1546.92 nm) and a tunable external-cavity laser diode (Sacher TEC 500, 1380–1520 nm) were used as light sources. An example of the measured spectra is shown in Figure 1. The lines are labelled according to the notation used in reference [16].

By synchronizing the ring down acquisition with the microwave pulse, time resolved spectroscopy can be achieved with time resolution commensurate with the ring down time (typically ~ 32 μs).

3 Theoretical calculations

The measured absorption lines were fitted by a Voigt profile and the obtained line positions (ν_{exp}) are listed in Table 1 together with calculated theoretical values (ν_{calc}). In the calculations we used an effective Hamiltonian for $^3\Sigma$ and $^3\Pi$ states [17] with matrix elements from reference [18] including selection rules and symmetry restrictions [19]. Note that the matrix elements listed in reference [18] are for the $^3\Sigma^-$ state. The matrix elements for the $^3\Sigma^+$ state are the same, except that f is replaced by e and e is replaced by f. The spectroscopic constants for $v = 0$ and $v = 1$ vibrational states of $a^3\Sigma_u^+$ and $b^3\Pi_g$ were taken from reference [16], while those for the $v = 2$ vibrational state of $b^3\Pi_g$ were partly taken from reference [20] and partly set to be the same as for the $v = 1$ state.

To obtain the number densities of different states of He_2 we followed the procedure described by Tokaryk et al. [21]. We used potential energy curves for $a^3\Sigma_u^+$ and $b^3\Pi_g$ electronic states calculated by Yarkony [22] as an input into the program Level by Le Roy [23] for calculation of energy levels. The bound-states wavefunctions corresponding to the quantum numbers v and N were obtained as solutions of the Schrödinger equation using Numerov-Cooley methods [24,25] as implemented in reference [26]. The wavefunctions were then used together with the transition dipole moment function $\mu_\perp$ [22] connecting the given electronic states to calculate appropriate Einstein coefficients $A_{v'N'J'\to v''N''J''}$. A set of rotational line strength (Hönl-London) factors $S_{N'J',N''J''}$ [27] for an allowed $^3\Pi - {}^3\Sigma$ transition in Hund's case (b) with a given $N = N'$ (or N'') when normalized obey a sum rule $\sum S_{N'J',N''J''} = 6(2N + 1)$, with the sum over all $\Delta N = N' - N''$ and over the different components J' and J''. The calculated values of Einstein coefficients for a list of selected transitions are shown in Table 1.

The number density n_{He_2} of a particular state of He_2 was then determined using formula [28]:

$$n_{He_2} = 8\pi c\nu^2 \frac{2J''+1}{2J'+1} \frac{\sqrt{2\pi}\sigma_D}{A_{v'N'J'\to v''N''J''}} \xi \text{ [cm}^{-3}\text{]}, \quad (1)$$

where c is speed of light (in units of cm s^{-1}), ξ (cm^{-1}) is the absorption coefficient at the centre of the Doppler broadened absorption line (described by standard deviation σ_D (cm^{-1})), $A_{v'N'J'\to v''N''J''}$ (s^{-1}) is the Einstein coefficient for spontaneous emission of a photon with wavenumber ν (cm^{-1}), and J' and J'' are the rotational quantum numbers of the upper and lower state, respectively. At 80 K, the obtained number densities of the $v = 0$, $N = 1$, $J = 0$ $a^3\Sigma_u^+$ state of He_2 during the discharge were on the order of 10^9 cm^{-3} in 900 Pa of pure He and on the order of 10^7 cm^{-3} in a mixture of He/Ar/H_2. For example at $8\times10^{17}/1\times10^{14}/2\times10^{14}$ cm^{-3} and measured absorption coefficient at the centre of the absorption line $\xi = 3.2\times10^{-6}$ cm^{-1} (corresponding to $R_{23}(1)$ transition in Fig. 1), the obtained number density of $v = 0$, $N = 1$, $J = 0$ $a^3\Sigma_u^+$ state of He_2 is 1.1×10^7 cm^{-3}.

4 Results and discussion

One necessary condition for measuring a recombination rate coefficient of H_3^+ in SA-CRDS experiments is that the afterglow plasma has to be free from excited particles that may in superelastic collisions heat the electrons. It has been observed many times that in an afterglow plasma in He the presence of excited neutrals can be suppressed by a small admixture of a reactant gas which removes He and He_2 metastables by Penning ionization [29,30]. The time evolutions of the relative populations of He_2 (transitions $Q_{22}(1)$ and $R_{22}(27)$ originating from the

Table 1. Measured transitions (ν_{exp}) belonging to the (1–0) and (2–1) vibrational bands of the He_2 $b^3\Pi_g$–$a^3\Sigma_u^+$ system compared to the calculated values (ν_{calc}). The estimated error of the measurement is 5×10^{-3} cm^{-1}. The calculated Einstein coefficients of spontaneous emission A are also listed.

band	transition	ν_{exp}(cm^{-1})	ν_{calc}(cm^{-1})	A (10^4 s^{-1})	band	transition	ν_{exp}(cm^{-1})	ν_{calc}(cm^{-1})	A (10^4 s^{-1})
(2–1)	$R_{22}(15)$	6459.925	6459.918	13.8	(2–1)	$R_{22}(13)$	6462.464	6462.460	13.7
(2–1)	$R_{11}(15)$	6460.028	6460.024	13.9	(2–1)	$R_{11}(13)$	6462.565	6462.564	13.7
(2–1)	$R_{33}(15)$	6460.074	6460.072	13.9	(2–1)	$R_{33}(13)$	6462.615	6462.616	13.8
(2–1)	$R_{22}(11)$	6460.788	6460.785	13.5	(1–0)	$Q_{11}(1)^c$	6465.886	6465.890	9.6
(2–1)	$R_{11}(11)$	6460.888	6460.886	13.6	(1–0)	$R_{12}(1)^d$	6465.917	6465.919	3.0
(2–1)	$R_{33}(11)$	6460.943	6460.943	13.6	(1–0)	$P_{12}(1)$	6466.027	6466.026	6.1
(1–0)	$Q_{11}(3)$	6461.151	6461.154	11.3	(1–0)	$R_{23}(1)$	6466.216	6466.217	4.0
(1–0)	$Q_{33}(3)$	6461.190	6461.192	10.7	(1–0)	$P_{21}(1)$	6466.260	6466.261	5.0
(1–0)	$P_{32}(3)$	6461.234	6461.236	1.9	(1–0)	$Q_{22}(1)$	6466.289	6466.290	3.1
(1–0)	$R_{23}(3)^a$	6461.446	6461.444	1.0	(1–0)	$R_{22}(21)$	6533.661	6533.666	8.2
(1–0)	$P_{21}(3)^b$	6461.460	6461.456	1.0	(1–0)	$R_{11}(21)$	6533.765	6533.760	8.4
(1–0)	$Q_{22}(3)$	6461.488	6461.488	10.1	(1–0)	$R_{33}(21)$	6533.806	6533.811	8.2
(1–0)	$R_{22}(27)$	6462.260	6462.251	8.2	(1–0)	$R_{22}(5)$	6536.518	6536.518	7.2
(1–0)	$R_{11}(27)$	6462.369	6462.360	8.2	(1–0)	$R_{11}(5)$	6536.598	6536.599	7.5
(1–0)	$R_{33}(27)$	6462.407	6462.411	8.2	(1–0)	$R_{33}(5)$	6536.694	6536.694	7.2

[a]Blended with $P_{21}(3)$; [b]blended with $R_{23}(3)$; [c]blended with $R_{12}(1)$; [d]blended with $Q_{11}(1)$.

$a^3\Sigma_u^+(v = 0)$ electronic state) measured during the discharge and the afterglow in pure He are shown in Figure 2a. The decrease of the densities of both states is very slow and it is clear that highly excited He_2 are present even 1 ms after switching off the discharge. This is consistent with previously observed slow decrease of the electron temperature in He afterglow [30]. Detailed description of the processes involving atomic and molecular metastables in He buffered plasmas is given e.g., in reference [21].

Excited He and He_2 metastables can be removed from the afterglow plasma by adding Ar to the He buffer gas. The removal of metastable particles from the afterglow plasma by adding Ar leads to a decrease in electron temperature [30]. In the present study we observed the removal of He_2 and excited Ar ($3s^23p^5(^2P^\circ_{1/2})3d\ ^2[3/2]^\circ$, $J = 2$) on a microsecond scale in the He/Ar/H_2 mixture (see Fig. 3). This is substantially faster than the time scale of the electron density decrease in a plasma that is dominated by the recombination of H_3^+ ions at similar conditions (see Fig. 2b).

As there are several allowed transitions from the $3s^23p^5(^2P^\circ_{1/2})3d\ ^2[3/2]^\circ, J = 2$ excited state of argon to lower states with corresponding Einstein A coefficients on the order of 10^6 s^{-1} [32] the lifetime of the $3s^23p^5(^2P^\circ_{1/2})3d\ ^2[3/2]^\circ, J = 2$ state will be on the order of hundreds of nanoseconds or lower. As can be seen from Figure 3a, the $3s^23p^5(^2P^\circ_{1/2})3d\ ^2[3/2]^\circ, J = 2$ excited state of argon survives in the He/Ar mixture ($4.1 \times 10^{17}/2.1 \times 10^{13}$ cm^{-3}) after switching off the discharge substantially longer than what would have been expected from its lifetime. This indicates that another source of excitation energy is present as the energy difference between the $3s^23p^5(^2P^\circ_{1/2})3d\ ^2[3/2]^\circ, J = 2$ state and the ground state of argon is more than 14 eV. The most likely source of this energy are helium metastable atoms that are produced in the discharge. In the afterglow the helium metastable atoms are removed by Penning ionization of argon. With the rate coefficient $k_{PI} = 7 \times 10^{-11}$ cm^3 s^{-1} [33] and [Ar] $= 2.1 \times 10^{13}$ cm^{-3} the characteristic reaction time for Penning ionization of Ar by helium metastable atoms is $\approx$ 700 μs, i.e., similar to the time constant of the decay of the $3s^23p^5(^2P^\circ_{1/2})3d\ ^2[3/2]^\circ, J = 2$ excited state of argon in the afterglow plasma as shown by the dashed line in Figure 3a. At conditions used in H_3^+ recombination studies [31,34] the $3s^23p^5(^2P^\circ_{1/2})3d\ ^2[3/2]^\circ, J = 2$ state of argon is quickly removed from the afterglow (full line in Fig. 3a) indirectly hinting that also the helium metastable atoms are being destroyed.

We have performed several measurements of time evolutions of the absorption signals proportional to the number densities of the $3s^23p^5(^2P^\circ_{1/2})3d\ ^2[3/2]^\circ, J = 2$ state of argon and the $a^3\Sigma_u^+(v = 0)$, $N = 1$ state of He_2 in the discharge and in the afterglow plasma at different [Ar] and [H_2]. The results obtained at 140 K are plotted in Figure 4. As can be seen from Figure 4, the decay of the absorption signal is faster with increasing [H_2]. Similar dependence on [Ar] was also observed. We have evaluated the measured decay curves by fitting them with a single exponential decay. The dependences of the reciprocal values $1/\tau$ of the measured time constants τ of the exponential decays on [H_2] are plotted in the insert of Figure 4. The measured time constants for given states of Ar and He_2 are the same within the experimental errors in the probed range of [Ar] and [H_2] (for details see the insert of Fig. 4) indicating that metastable helium atoms probably serve as precursors for the creation of both He_2 and the $3s^23p^5(^2P^\circ_{1/2})3d\ ^2[3/2]^\circ, J = 2$ state of Ar in the afterglow. The corresponding rate coefficient for destruction of

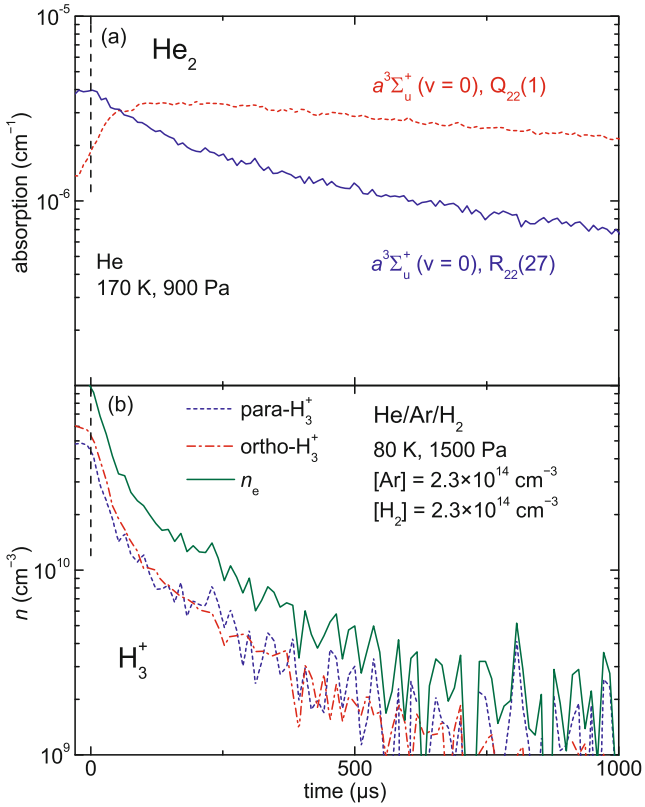

Fig. 2. (a) Time evolution of the absorption in the afterglow plasma measured at 170 K in 900 Pa of pure He using the transitions originating from the ground vibrational state (transitions $Q_{22}(1)$ and $R_{22}(27)$) of the $a^3\Sigma_u^+$ electronic state of the He_2 molecule. The upper state belongs to the first vibrational state of the $b^3\Pi_g$ electronic state of He_2. Unlike the $R_{22}(27)$ transition, we were not able to measure at the centre of the $Q_{22}(1)$ absorption line as the absorption was too strong, exceeding the limits of our spectrometer. The displayed time evolution of absorption was therefore measured slightly off the centre of the line (at 6466.362 cm^{-1} instead of 6466.289 cm^{-1}). The zero time is set at the beginning of the afterglow. (b) Time evolution of number densities of ortho-H_3^+ and para-H_3^+ ions measured in the afterglow plasma at 80 K in a $He/Ar/H_2$ mixture ($1.4\times10^{18}/2.3\times10^{14}/2.3\times10^{14}$ cm^{-3}). The electron number density (n_e) is calculated under the assumption of plasma quasineutrality and thermal population of states [31].

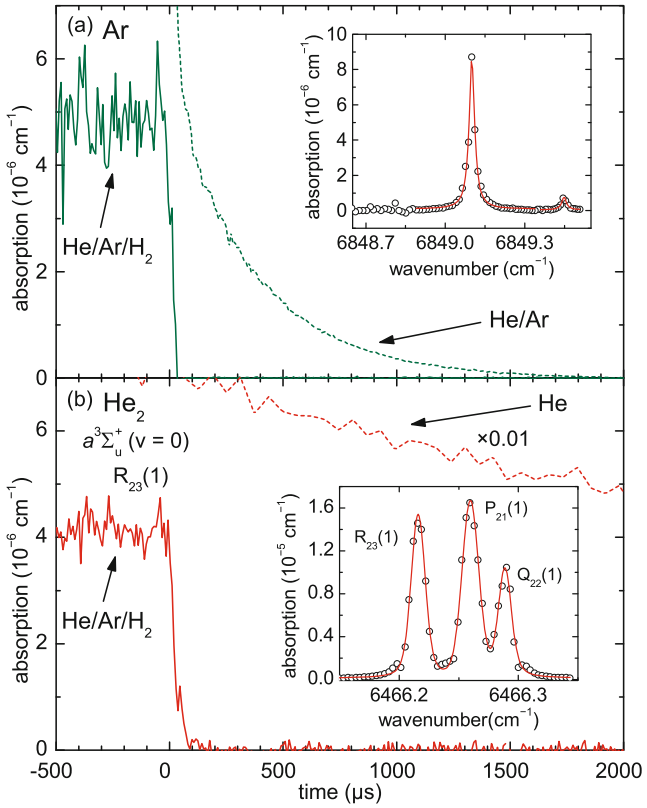

Fig. 3. (a) Time evolution of the absorption at the centre of an Ar absorption line (transition $3s^23p^5(^2P^\circ_{1/2})3d\ ^2[3/2]^\circ$, $J = 2 \rightarrow 3s^23p^5(^2P^\circ_{1/2})4f\ ^2[5/2]$, $J = 3$; 6849.099 cm^{-1} [32,35]). The full and dashed lines denote the data measured at 80 K in a $He/Ar/H_2$ mixture ($8.3\times10^{17}/3.4\times10^{14}/2.7\times10^{14}$ cm^{-3}) and in a He/Ar mixture ($4.1\times10^{17}/2.1\times10^{13}$ cm^{-3}), respectively. Note that in He/Ar the characteristic reaction time for Penning ionization of Ar by helium metastable atoms is ≈ 700 μs (with $k_{PI} = 7\times10^{-11}$ $cm^3\ s^{-1}$ [33]). The insert shows the corresponding absorption line profile. (b) Time evolution of the absorption at the centre of a He_2 absorption line (transition $R_{23}(1)$ in the (1–0) vibrational band of the $b^3\Pi_g - a^3\Sigma_u^+$ system). The full and dashed lines denote the data obtained at 80 K in a $He/Ar/H_2$ mixture ($7.6\times10^{17}/2.9\times10^{14}/2.5\times10^{14}$ cm^{-3}) and in pure He (8.1×10^{17} cm^{-3}) (scaled by a factor of 0.01 to fit into the figure), respectively. The insert shows the corresponding absorption line profiles.

helium metastable atoms (states $2\,^1S$ and $2\,^3S$) in collisions with H_2 at 140 K evaluated from the slope of the linear fit to the data in the insert of Figure 4 is $k_M(140\ K) = (1.9 \pm 0.2)\times10^{-10}$ $cm^3\ s^{-1}$. Similar analysis was also done for values obtained at 80 K and 300 K with resulting rate coefficients of $k_M(80\ K) = (0.9\pm0.3)\times10^{-10} cm^3\ s^{-1}$ and $k_M(300\ K) = (2.7\pm0.2)\times10^{-10} cm^3\ s^{-1}$. These values are close to the values reported in the literature [36–38]. Based on the measurements shown in Figure 4 we can estimate the densities of Ar and H_2 that are needed to remove the excited particles from the afterglow within 100 μs after switching off the discharge as required for our studies of recombination of H_3^+ ions (see Fig. 3).

In the present experiments using $He/Ar/H_2$ gas mixtures we measured the decay of H_3^+ ion density (decay curve) by monitoring absorption of three states ((1,1) of para-H_3^+ and (1,0) and (3,3) of ortho-H_3^+, for details on notation see Ref. [39]). The kinetic temperature of H_3^+ ions ($T_{kin\text{-}ion}$) was measured from the Doppler broadening of the absorption line profiles [31]. The rotational temperature (T_{rot}) and the ratio of densities of para-H_3^+ to ortho-H_3^+ were determined from measured partial populations of ions in the lowest rotational states of the vibrational ground state of H_3^+ [31]. On the basis of our measurements we conclude that for the afterglow plasmas in $He/Ar/H_2$ in the SA-CRDS experiments the $T_{kin\text{-}ion}$ and T_{rot} of ions are

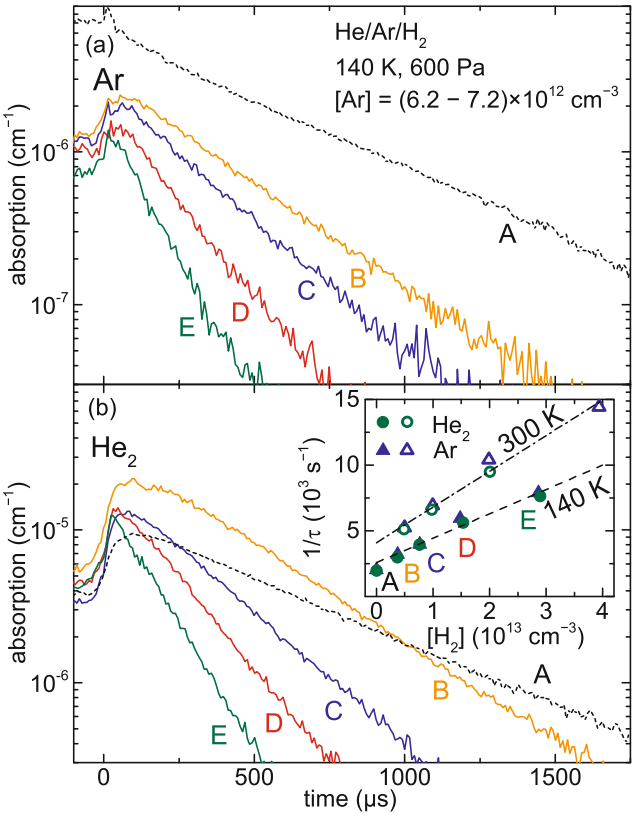

Fig. 4. (a) Time evolutions of the absorption coefficient measured at the centre of an argon absorption line (transition $3s^2 3p^5(^2P^\circ_{1/2})3d\ ^2[3/2]^\circ, J = 2 \rightarrow 3s^2 3p^5(^2P^\circ_{1/2})4f\ ^2[5/2], J = 3$; 6849.099 cm^{-1} [32,35]) in the discharge and the afterglow plasma, at [He] = 3.1×10^{17} cm^{-3}, [Ar] ≈ 6.7×10^{12} cm^{-3}, and different densities of H_2, capital letters A, B, C, D, and E indicate [H_2] = 0, 3.8, 7.6, 15, and 29×10^{12} cm^{-3}, respectively. The time is set to zero at the beginning of the afterglow. (b) Time evolutions of the absorption coefficient measured slightly off the centre of an He_2 absorption line (transition $R_{23}(1)$, measured at 6466.196 cm^{-1} instead of 6466.216 cm^{-1}, because of too high absorption at the centre of the absorption line) in the discharge and the afterglow plasma, at the same conditions as in panel (a). Insert: The [H_2] dependences of the measured pseudo-first-order rate coefficients (reciprocal time constants $1/\tau$) of the exponential decays displayed in panels (a) (full triangles) and (b) (full circles). Capital letters A–E indicate corresponding [H_2]. For comparison the values of the same rate coefficients measured at 300 K and [He] = 2.2×10^{17} cm^{-3} and [Ar] = 7×10^{12} cm^{-3} for Ar (open triangles) and He_2 (open circles) are also plotted. The dashed and dot-dashed straight lines are fits to the measured pseudo-first-order rate coefficients at 140 K and 300 K, respectively.

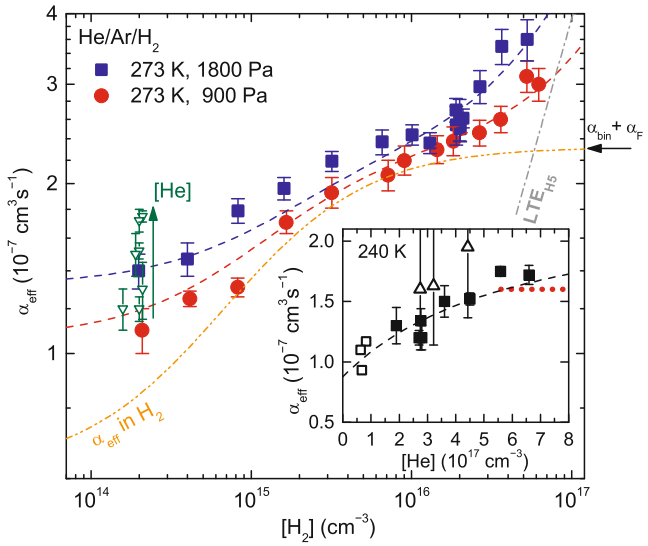

Fig. 5. Dependences of $\alpha_{\rm eff}$ on [H_2] measured at 273 K (the data were adapted from Ref. [12]). The dashed lines are fits to the data by equation (4) extended by the term accounting for H_5^+ formation. The double dot dashed line ($\alpha_{\rm eff}$ in H_2) denotes the effective recombination rate coefficient $\alpha_{\rm eff}$ that would have been measured in pure H_2. The dot-dashed straight line (LTE_{H5}) is the calculated upper limit of the contribution from H_5^+ formation (see Refs. [11,12]). The open triangles indicate the data measured in this experiment at fixed [H_2] ≈ 2×10^{14} cm^{-3} and different values of [He], the arrow indicates the increase of $\alpha_{\rm eff}$ with increasing [He]. Insert: Measured dependence of $\alpha_{\rm eff}$ on [He] (full squares) at 240 K compared to the values obtained in our previous SA (open squares) and FALP (open triangles) experiments [7]. The dashed line denotes the fit to the data by equation (4). The dotted line denotes the values measured by MacDonald [6] in neon at [Ne] = $5.6 \times 10^{17} - 8 \times 10^{17}$ cm^{-3}.

equal to the temperature of the helium buffer gas ($T_{\rm He}$) and the wall temperature ($T_{\rm wall}$) of the discharge tube, i.e., we can write: $T = T_{\rm wall} = T_{\rm He} = T_{\rm rot} = T_{\rm kin\text{-}ion}$ (for details see Ref. [31]). The electron temperature $T_{\rm e}$ was not measured in the present study (see discussion in Ref. [31]). At He densities typical for the present experiments the estimated characteristic time of the electron cooling in collisions with He atoms is below 10 μs.

An example of ion density decay curves of para-H_3^+ and ortho-H_3^+ measured at 80 K in a mixture of He/Ar/H_2 is plotted in Figure 2b. Because of the fast removal of He and He_2 metastables and Ar excited states in the used He/Ar/H_2 mixture (see Fig. 3) we can expect that the afterglow plasma dominated by H_3^+ recombination is in thermal equilibrium. From the measured decrease of ion densities during the afterglow the effective binary recombination rate coefficient $\alpha_{\rm eff}$ can be calculated [31]. In systematic studies of dependence of $\alpha_{\rm eff}$ on [He] and [H_2] we obtained dependences $\alpha_{\rm eff}(T, [{\rm He}], [{\rm H_2}])$. Examples of typical data are plotted in Figure 5.

To understand the measured dependences $\alpha_{\rm eff}(T, [{\rm He}], [{\rm H_2}])$, we propose a model where we consider binary recombination process:

$$H_3^+ + e^- \xrightarrow{\alpha_{\rm bin}} \text{neutral}, \qquad (2)$$

where $\alpha_{\rm bin}$ is the rate coefficient of binary dissociative recombination. We also consider ternary neutral assisted recombination, where we postulate formation of highly excited $H_3^\#$ "complexes" that can either decay by

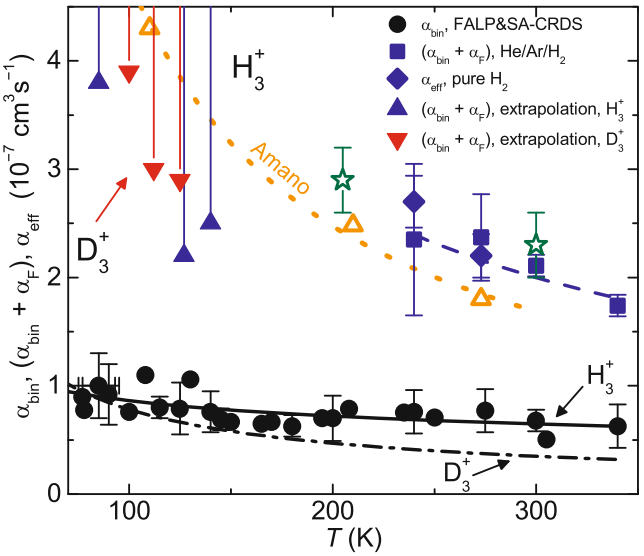

Fig. 6. Binary rate coefficient $\alpha_{\rm bin}$ and the sum of $(\alpha_{\rm bin}+\alpha_{\rm F})$ characterizing the recombination of H_3^+ in low temperature plasmas. The lowest boundary estimates of $(\alpha_{\rm bin}+\alpha_{\rm F})$ (filled up-triangles) were obtained from the maxima of measured linear dependences of $\alpha_{\rm eff}$ of H_3^+ ions on [He]. The filled down-triangles denote the lowest boundary estimates of $(\alpha_{\rm bin}+\alpha_{\rm F})$ obtained for D_3^+ (compilation of data from Ref. [40]). The open triangles indicate values of $\alpha_{\rm eff}$ measured by Amano [10] in pure H_2 gas. The dotted line is a fit to Amano's values: $\alpha_{\rm Amano} = 1.7\times10^{-7}(T/300\ {\rm K})^{-0.94}$ cm^3 s^{-1}. The stars show the values of $\alpha_{\rm eff}$ obtained by Leu et al. [9] in high pressure stationary afterglow experiments. The diamonds and squares denote the values of $\alpha_{\rm eff}$ measured by Glosík et al. [12] in pure H_2 gas and in a mixture of He/Ar/H_2 with $[H_2] > 2\times10^{16}$ cm^{-3}, respectively, these values are fitted by the dashed line [12]. The full and dot dashed lines are the fits to the values of $\alpha_{\rm bin}$ of H_3^+ (full circles) and D_3^+ ions (only the fit is indicated, the data were taken from Ref. [41]), respectively.

autoionization or can be stabilized in collisions with He or H_2:

$$H_3^+ + e^- \underset{\tau_a}{\overset{\alpha_F}{\rightleftarrows}} H_3^\# \underset{k_{SH_2}}{\overset{k_{SHe}}{\rightrightarrows}} \text{neutral}, \qquad (3)$$

where $\alpha_{\rm F}$ is the binary rate coefficient for formation of $H_3^\#$, $\tau_{\rm a}$ is the autoionization time constant, and $k_{\rm SHe}$ and $k_{\rm SH_2}$ are the binary rate coefficients for stabilization of $H_3^\#$ in collisions with He and H_2, respectively. By writing the balance equations and by introducing $K_{\rm He} = \alpha_{\rm F} k_{\rm SHe}\tau_{\rm a}$ and $K_{H_2} = \alpha_{\rm F} k_{\rm SH_2}\tau_{\rm a}$ we can obtain for $\alpha_{\rm eff}$ (for details see Ref. [12]):

$$\alpha_{\rm eff} = \alpha_{\rm bin} + \alpha_{\rm F}\frac{K_{\rm He}[{\rm He}] + K_{H_2}[H_2]}{\alpha_{\rm F} + K_{\rm He}[{\rm He}] + K_{H_2}[H_2]}. \qquad (4)$$

At high [He] and/or $[H_2]$ densities the measured $\alpha_{\rm eff}$ saturates at a value of $\alpha_{\rm eff} = (\alpha_{\rm bin}+\alpha_{\rm F})$. In the low density limit ([He] and $[H_2] \to 0$) equation (4) reduces to linear dependence $\alpha_{\rm eff} = \alpha_{\rm bin} + K_{\rm He}[{\rm He}] + K_{H_2}[H_2]$. The measured $\alpha_{\rm eff}(T, [{\rm He}], [H_2])$ are fitted by formula (4) extended by the term accounting for formation of H_5^+ ions and their consequent recombination [12]. From the fits of data measured over a sufficiently broad range of He and H_2 densities the values of $\alpha_{\rm bin}$, $\alpha_{\rm F}$, $K_{\rm He}$, and K_{H_2} can be determined. The obtained values of the binary recombination rate coefficient $\alpha_{\rm bin}$ and the values of $(\alpha_{\rm bin}+\alpha_{\rm F})$ are shown in Figure 6.

Under our present experimental conditions at temperatures below 240 K the losses of H_3^+ ions due to the formation of H_5^+ dominate at high [He] and $[H_2]$ over losses due to the ternary recombination, and from the measured dependence of $\alpha_{\rm eff}$ on [He] (see insert in Fig. 5) only a lower limit for the value of $(\alpha_{\rm bin}+\alpha_{\rm F})$ can be estimated. In Figure 6 we included these lower limits obtained in our experiments with H_3^+ at low temperatures. For comparison we also plotted lower limits obtained for D_3^+ from the compilation of data measured in our previous experiments [40]. The ternary recombination rate coefficients $K_{\rm He}$ and K_{H_2} and their temperature dependence (in the range of 240–340 K) are discussed in our previous publication (see Ref. [12]).

5 Conclusion

We have studied plasma thermalization during the afterglow using a stationary afterglow apparatus equipped with CRDS absorption spectrometer (SA-CRDS) from 77 K up to 340 K in pure He, and in He/Ar and He/Ar/H_2 gas mixtures. We confirmed our previous conclusions that at conditions used in our studies of H_3^+ recombination the afterglow plasma is thermalized. The present values of $\alpha_{\rm bin}$ and $(\alpha_{\rm bin}+\alpha_{\rm F})$ are consistent with our previous data. Further experiments in pure H_2 at higher electron densities are required to obtain $(\alpha_{\rm bin}+\alpha_{\rm F})$ and K_{H_2} at temperatures below 240 K.

This work was partly supported by Czech Science Foundation projects GACR 15-15077S, GACR 14-14649P, and by Charles University Grant Agency project GAUK 692214. We would like to thank Professor Rainer Johnsen for fruitful discussions.

References

1. T. Oka, Proc. Natl. Acad. Sci. USA **103**, 12235 (2006)
2. T.J. Millar, Plasma Source. Sci. Technol. **24**, 043001 (2015)
3. M. Larsson, A.E. Orel, *Dissociative Recombination of Molecular Ions* (Cambridge University Press, Cambridge, 2008)
4. H. Kreckel et al., Phys. Rev. Lett. **95**, 263201 (2005)
5. B.J. McCall et al., Nature **422**, 500 (2003)
6. J.A. Macdonald, M.A. Biondi, R. Johnsen, Planet. Space Sci. **32**, 651 (1984)
7. J. Glosík, R. Plašil, I. Korolov, T. Kotrík, O. Novotný, P. Hlavenka, P. Dohnal, J. Varju, V. Kokoouline, C.H. Greene, Phys. Rev. A **79**, 052707 (2009)
8. N.G. Adams, D. Smith, E. Alge, J. Chem. Phys. **81**, 1778 (1984)

9. M.T. Leu, M.A. Biondi, R. Johnsen, Phys. Rev. A **8**, 420 (1973)
10. T. Amano, J. Chem. Phys. **92**, 6492 (1990)
11. P. Dohnal, P. Rubovič, Á. Kálosi, M. Hejduk, R. Plašil, R. Johnsen, J. Glosík, Phys. Rev. A **90**, 042708 (2014)
12. J. Glosík, P. Dohnal, P. Rubovič, Á. Kálosi, R. Plašil, Š. Roučka, R. Johnsen, Plasma Source. Sci. Technol. **24**, 065017 (2015)
13. D.R. Bates, S.P. Khare, Proc. Phys. Soc. **85**, 231 (1965)
14. P. Macko, G. Bánó, P. Hlavenka, R. Plašil, V. Poterya, A. Pysanenko, O. Votava, R. Johnsen, J. Glosík, Int. J. Mass Spectrom. **233**, 299 (2004)
15. D. Romanini, A.A. Kachanov, N. Sadeghi, F. Stoeckel, Chem. Phys. Lett. **264**, 316 (1997)
16. C. Focsa, P.F. Bernath, R. Colin, J. Mol. Spectrosc. **191**, 209 (1998)
17. J.M. Brown, E.A. Colbourn, J.K.G. Watson, F.D. Wayne, J. Mol. Spectrosc. **74**, 294 (1979)
18. C.R. Brazier, R.S. Ram, P.F. Bernath, J. Mol. Spectrosc. **120**, 381 (1986)
19. L. Augustovičová, V. Špirko, W.P. Kraemer, P. Soldán, MNRAS **435**, 1541 (2013)
20. M.L. Ginter, J. Mol. Spectrosc. **18**, 321 (1965)
21. D.W. Tokaryk, R.L. Brooks, J.L. Hunt, Phys. Rev. A **48**, 364 (1993)
22. D.R. Yarkony, J. Chem. Phys. **90**, 7164 (1989)
23. R.J. Le Roy, LEVEL 7.7: A Computer Program for Solving the Radial Schrodinger Equation, University of Waterloo Chemical Physics Research Report CP-661, 2005
24. B. Numerov, Trudy Glavnoi Rossiskoi Astrofizicheskoi Observatorii **2**, 188 (1923)
25. J.W. Cooley, Math. Comp. **15**, 363 (1961)
26. L. Augustovičová, V. Špirko, W.P. Kraemer, P. Soldán, Astron. Astrophys. **553**, A42 (2013)
27. J.K.G. Watson, J. Mol. Spectrosc. **252**, 5 (2008)
28. L.S. Rothman et al., J. Quant. Spectrosc. Radiat. Transfer **60**, 665 (1998)
29. R. Plašil, I. Korolov, T. Kotrík, P. Dohnal, G. Bánó, Z. Donkó, J. Glosík, Eur. Phys. J. D **54**, 391 (2009)
30. I. Korolov, R. Plašil, T. Kotrík, P. Dohnal, O. Novotný, J. Glosík, Contrib. Plasma Phys. **48**, 461 (2008)
31. M. Hejduk, P. Dohnal, P. Rubovič, Á. Kálosi, R., Plašil, R. Johnsen, J. Glosík, J. Chem. Phys. **143**, 044303 (2015)
32. W.L. Wiese, J.M. Bridges, R.L. Kornblith, D.E. Kelleher, J. Opt. Soc. Am. **59**, 1206 (1969)
33. J. Glosík, G. Bánó, R. Plašil, A. Luca, P. Zakouřil, Int. J. Mass Spectrom. **189**, 103 (1999)
34. P. Dohnal, M. Hejduk, J. Varju, P. Rubovič, Š. Roučka, T. Kotrík, R. Plašil, J. Glosík, R. Johnsen, J. Chem. Phys. **136**, 244304 (2012)
35. P. Palmeri, E. Biémont, Phys. Scr. **51**, 76 (1995)
36. M.H. Nayfeh, C.H. Chen, M.G. Payne, Phys. Rev. A **14**, 1739 (1976)
37. W. Lindinger, A.L. Schmeltekopf, F.C. Fehsenfeld, J. Chem. Phys. **61**, 2890 (1974)
38. A.L. Schmeltekopf, F.C. Fehsenfeld, J. Chem. Phys. **53**, 3173 (1970)
39. C.M. Lindsay, B.J. McCall, J. Mol. Spectrosc. **210**, 60 (2001)
40. P. Dohnal, M. Hejduk, P. Rubovič, J. Varju, Š. Roučka, R. Plašil, J. Glosík, J. Chem. Phys. **137**, 194320 (2012)
41. P. Rubovič, P. Dohnal, M. Hejduk, R. Plašil, J. Glosík, J. Phys. Chem. A **117**, 9626 (2013)